Peer-reviewed version available at Viruses 2018, 10, 726; doi:10.3390/v10120726

Article

The amino-terminal region of hepatitis E virus ORF1 containing a methyltransferase (Met) and a papain-like cysteine protease (PCP) domain counteracts type I interferon response.

Eugénie Bagdassarian[1,2,3#], Virginie Doceul[1,2,3#*], Marie Pellerin[1,2,3], Antonin Demange[1,2,3§], Léa Meyer[1,2,3], Nolwenn Jouvenet[4], Nicole Pavio[1,2,3].

[1] Anses, UMR 1161 Virologie, Laboratoire de santé animale, Maisons-Alfort, France; eugenie.bagdassarian@gmail.com (E.B.); marie.pellerin@anses.fr (M.P.); antonin.demange@ird.fr (A.D.); lea.meyer@vet-alfort.fr (L.M.); nicole.pavio@anses.fr (N.P.)
[2] INRA, UMR 1161 Virologie, Maisons-Alfort, France
[3] École Nationale Vétérinaire d'Alfort, UMR 1161 Virologie, Maisons-Alfort, France
[4] CNRS-UMR3569, Unité de Génomique Virale et Vaccination, Institut Pasteur, Paris, France; nolwenn.jouvenet@pasteur.fr (N.J.)
§ Current address: UMR CNRS 5290, IRD 224, Université de Montpellier, Montpellier, France.
* Correspondence: virginie.doceul@vet-alfort.fr (V.D.); Tel.: +33-1-439-67372
# E.B. and V.D. contributed equally to this work

Abstract: Hepatitis E virus (HEV) is responsible for large waterborne epidemics of hepatitis in endemic countries and is an emerging zoonotic pathogen worldwide. In endemic regions, HEV-1 or HEV-2 genotypes are frequently associated with fulminant hepatitis in pregnant women, while with zoonotic HEV (HEV-3 and HEV-4), chronic cases of hepatitis and severe neurological disorders are reported. Hence, it is important to characterize the interactions between HEV and its host. Here, we investigated the ability of the non-structural polyprotein encoded by the first open reading frame (ORF1) of HEV to modulate the host early antiviral response and in particular the type I interferon (IFN-I) system. We found that the amino-terminal region of HEV-3 ORF1 (MetPCP), containing a putative methyltransferase (Met) and a papain-like cysteine protease (PCP) functional domain, inhibited IFN-stimulated response element (ISRE) promoter activation and the expression of several IFN-stimulated genes (ISGs) in response to IFN-I. We showed that the MetPCP domain interfered with the Janus kinase (JAK)/signal transducer and activator of transcription protein (STAT) signalling pathway by inhibiting STAT1 nuclear translocation and phosphorylation after IFN-I treatment. By contrast, MetPCP had no effect on STAT2 phosphorylation and a limited impact on the activation of the JAK/STAT pathway after IFN-II stimulation. This inhibitory function seemed to be genotype-dependent as MetPCP from HEV-1 had no significant effect on the JAK/STAT pathway. Overall, this study provides evidence that the predicted MetPCP domain of HEV ORF1 antagonises STAT1 activation to modulate the IFN response.

Keywords: hepatitis E virus; innate immunity; interferon response; JAK/STAT pathway; zoonosis; emerging pathogen.

1. Introduction

Hepatitis E virus (HEV) is a single stranded positive RNA virus belonging to the *Orthohepevirus* genus within the *Hepeviridae* family [1]. Its genome is 7.2 kb in length and codes for 3 open reading frames (ORF1 to 3) [2]. *ORF1* codes for a non-structural polyprotein composed of several putative functional domains including a methyltransferase (Met), a domain of unknown function (Y), a papain-like cysteine protease (PCP), a macro domain (X), a helicase and a RNA-dependent RNA polymerase (RdRp) [3]. It is still unclear whether ORF1 is expressed as a single polyprotein or cleaved to several functional proteins in the context of infection. Multiple studies have suggested that ORF1 is cleaved into several products [4–8] whereas a few others have reported a lack of processing of the viral polyprotein [9–11]. The use of different expression systems may explain these conflicting results. Recently, a paper has suggested that ORF1 is cleaved by thrombin and factor Xa [12]. *ORF2* and ORF3 code for the capsid protein and a multifunctional phosphoprotein, respectively. Four genotypes infect humans. Genotypes 1 and 2 (HEV-1 and HEV-2) are transmitted via the faecal-oral route, through the consumption of contaminated water or soiled food in endemic regions. In contrast, genotypes 3 and 4 (HEV-3 and HEV-4) are detected in humans and other animal species worldwide and are transmitted via direct contacts with infected animals or the consumption of infected meat [13,14]. In most human cases, HEV infection causes an acute hepatitis that is self-limited. However, fulminant hepatic failure can occur in pregnant women in endemic region (HEV-1 or -2), in patients with underlying chronic liver disease or in the elderly (HEV-3 or -4). More recently, chronic cases of hepatitis E have been reported in immunocompromised patients (HEV-3 or HEV-4) and extrahepatic manifestations including renal, pancreatic and neurological disorders have been linked to HEV infection [15]. With the exception of China, no country has yet commercialized an HEV vaccine and no treatment against HEV infection is approved.

Interferons (IFNs) are a group of secreted cytokines that play a key role in the host early antiviral response. Type I IFNs (IFN-I), composed mainly of IFN-α and –β, are produced directly in response to viral infection, upon sensing of viral molecular signatures by specialized cellular receptors such as retinoic-acid-inducible gene (RIG)-I-like receptors (RLRs) and Toll-like receptors (TLRs). IFN-I subsequently binds to IFN-α/β receptors (IFNAR) at the cell surface and activates the Janus kinase (JAK)/signal transducer and activator of transcription protein (STAT) signalling pathway in an autocrine and paracrine manner. Binding of IFN-I to its receptor leads to the phosphorylation of tyrosine kinase 2 (TYK2) and JAK1 [16–18] and the subsequent phosphorylation of the cytoplasmic domain of the IFNAR subunits [18–22]. STAT1 and STAT2 are then recruited and phosphorylated by the JAK kinases on tyrosine 701 and tyrosine 690, respectively [18,23]. Phosphorylated STAT1/STAT2 heterodimers are released in the cytoplasm where they interact with IFN response factor 9 (IRF9) to form IFN-stimulated gene (ISG) factor 3 (ISGF3). This transcription factor translocates to the nucleus where it binds to specific promoter elements called IFN-stimulated response element (ISRE), leading to the up-regulation of hundreds of IFN-stimulated genes (ISGs) that may display antiviral properties and contribute to the establishment of a rapid and robust antiviral state within the cell [24]. Most cells can produce IFN-I. In contrast, type II IFN (IFN-γ) is secreted mainly by activated T cells and natural killer cells. Binding of the cytokine to a specific IFN-γ receptor (IFNGR) leads to the phosphorylation of JAK1 and JAK2 and the subsequent phosphorylation of STAT1. STAT1 homodimers are then formed and translocate to the nucleus where they bind to specific promoters to activate the transcription of a different subset of ISGs [25].

Different reports suggest that an IFN response is triggered by HEV as the expression of IFN-I and multiple ISGs has been detected after infection *in vivo* and *in vitro* [26–31]. However, IFN-I seems to have a moderate and delayed antiviral effect on HEV infection *in vitro* and in patients, in comparison, for instance, to hepatitis C virus (HCV), another hepatotropic RNA virus [32,33]. Consistently, recent studies indicate that the host ISG response to IFN-I is inhibited during HEV infection [31–34] but the mechanisms involved in this inhibition remain poorly characterized. As a non-structural polyprotein, HEV ORF1 contains one or several functional domains able to modulate the IFN-I system. The macrodomain, the PCP domain and the Met domain were described as antagonists of the signalling cascade leading to IFN [35,36]. However, nothing is known about the ability of the viral polyprotein to inhibit the response to IFN-I and the JAK/STAT pathway. To address this question, we studied the effect of HEV ORF1 and several of its domains on this signalling

pathway. We used a transfected cell model to express full-length or fragments of ORF1 fused to a FLAG tag as it is difficult to detect the polyprotein and its putative cleavage products in the context of infection or replication [10,37]. We were particularly interested in testing PCP and the macrodomain (X) as such functional domains encoded by several RNA-positive viruses have been shown to modulate the host innate immune response [38–43]. The amino-terminal end of ORF1 (MetPCP) containing Met, Y and PCP was also included in this study as a putative zinc finger domain is present in Met that might be critical for the enzymatic activity of PCP [44]. We found that the MetPCP domain inhibited ISRE promoter activation and the expression of several ISGs after stimulation with IFN-I. Further investigations revealed that MetPCP interfered with STAT1 nuclear translocation and phosphorylation. Overall, our data provides evidence that the predicted MetPCP domain of HEV ORF1 antagonises STAT1 activation to modulate the IFN response.

2. Materials and Methods

2.1. Cells

Human embryonic kidney 293T cells were grown in DMEM supplemented with 10% heat-inactivated fetal calf serum (FCS), 1% pyruvate and 100 IU/ml penicillin and 100 µg/ml streptomycin (PS). Cells were maintained at 37°C in 95% air/5% CO_2.

2.2. HEV ORF1 cloning and plasmid constructs

The serum of a French patient suffering from severe hepatitis E was provided by the former Reference National Centre for HEV (HIA Val de Grâce, Paris). A strain of HEV-3f was extracted from this sample using QiAmp viral RNA kit (Qiagen). Reverse transcription-PCR (RT-PCR) was performed with a Primescript reverse transcriptase (Takara, Ozyme). A total of seven overlapping fragments were amplified using the hot start high-fidelity Phusion polymerase (Finnzymes, Ozyme) or a 5'RACE and 3' RACE kit (Invitrogen, Life Technologies) and cloned into the plasmid pCR2.1. The 7 overlapping fragments were then digested with restriction enzymes and ligated 2 by 2 with the T4 DNA ligase (Takara, Ozyme) to generate a DNA fragment corresponding to the full-length viral genome downstream of a T7 promoter and a unique SwaI restriction site. This fragment was subsequently cloned into a pUC19 vector to generate pUC19-FR-HuFulHEV3f. The complete nucleotide sequence coding for ORF1 was then determined by sequencing and deposited in the GenBank database under accession number MG197988. The position of the different putative functional domains of ORF1 was identified by comparison with a previous computer-based analysis [3]. DNA sequences coding for full-length ORF1 as well as MetPCP, Y, PCP, X, Met, MetY and YPCP (Figure 1A) were amplified using pUC19-FR-HuFulHEV3f as a template and specific primers (Table 1) by standard PCR using the Phusion high-fidelity DNA polymerase (Thermo Scientific). The PCR products were then cloned by *in vitro* recombination into pDONR207 (Gateway system, Invitrogen) as described previously [45]. These coding sequences were subsequently recombined into a translation optimized pCINeo-3×FLAG expression vector [46] using the Gateway cloning procedure (Invitrogen).

Gene product	Primers
ORF1	**F :** GGGGACAACTTTGTACAAAAAAGTTGGCATGGAGGCCCACCAGTTCATT **R :** GGGGACAACTTTGTACAAGAAAGTTGGTCATTCCAACCTCTGTATGAT
Met	**F :** GGGGACAACTTTGTACAAAAAAGTTGGCATGGAGGCCCACCAGTTCATT **R :** GGGGACAACTTTGTACAAGAAAGTTGGTTAGATCCATGCACGAAGTATAG
Y	**F :** GGGGACAACTTTGTACAAAAAAGTTGGCCGCGCCGTCGTGACTTATGAG **R :** GGGGACAACTTTGTACAAGAAAGTTGGTTAGCACTGTGCATAAAACTGTAG
PCP	**F :** GGGGACAACTTTGTACAAAAAAGTTGGCCAGTGCCGCCGCTGGCTCTCA **R :** GGGGACAACTTTGTACAAGAAAGTTGGTTACAAAACATACTGTTCGGGACCGTTG
MetPCP	**F :** GGGGACAACTTTGTACAAAAAAGTTGGCATGGAGGCCCACCAGTTCATT **R :** GGGGACAACTTTGTACAAGAAAGTTGGTTACAAAACATACTGTTCGGGACCGTTG
X	**F :** GGGGACAACTTTGTACAAAAAAGTTGGCGCCCGCACTCGCCGGCTCCTT **R :** GGGGACAACTTTGTACAAGAAAGTTGGTTAGCCGGCGCAAGCACGACCCAC
MetY	**F :** GGGGACAACTTTGTACAAAAAAGTTGGCATGGAGGCCCACCAGTTCATT **R :** GGGGACAACTTTGTACAAGAAAGTTGGTTAGCACTGTGCATAAAACTGTAG
YPCP	**F :** GGGGACAACTTTGTACAAAAAAGTTGGCCGCGCCGTCGTGACTTATGAG **R :** GGGGACAACTTTGTACAAGAAAGTTGGTTACAAAACATACTGTTCGGGACCGTTG
MetPCP (HEV-1)	**F :** GGGGACAACTTTGTACAAAAAAGTTGGCATGGAGGCCCATCAGTTTATCAAG **R :** GGGGACAACTTTGTACAAGAAAGTTGGTTAAAGATTGTGGCGCTCCGGGC
PCP (HEV-1)	**F :** GGGGACAACTTTGTACAAAAAAGTTGGCCAGTGTAGGCGCTGGCTTTCG **R :** GGGGACAACTTTGTACAAGAAAGTTGGTTAAAGATTGTGGCGCTCCGGGC
ISG56	**F :** GGACAGGAAGCTGAAGGAG **R :** AGTGGGTGTTTCCTGCAA
MDA5	**F :** ACACGTTCTTTGCGATTTCC **R :** ACCAAATACAGGAGCCATGC
OAS1	**F :** CATCCGCCTAGTCAAGCACTG **R :** CACCACCCAAGTTTCCTGTAG
GADPH	**F :** GGTCGGAGGTCAACGGATTTG **R :** ACTCCACGACGTACTCAGCG

Table 1. Primers used for the amplification of DNA sequences coding for full-length or fragments of HEV-3 and HEV-1 ORF1 and for the quantification of ISG expression by RT-qPCR. F: forward primer, R: reverse primer.

A similar strategy was used to construct the plasmid coding for 3×FLAG-tagged MetPCP and PCP from HEV-1. RNA from a HEV-1 strain was extracted from a stool sample of a patient with acute hepatitis provided by the previous Reference National Centre for HEV (HIA Val de Grâce, Paris) using a RNeasy kit (Qiagen). Reverse transcription was then performed with the PrimeScript Reverse Transcriptase (Takara Bio USA, Inc. CA, USA) according to the manufacturer's protocol. Three overlapping fragments covering the ORF1 region were amplified using Ex Taq polymerase (Takara Bio Inc. Shiga) and inserted into TOPO pCR2.1 using the TOPO TA cloning kit (Invitrogen Life technologies). These 3 constructs were sequenced and used as template to amplify sequences coding for MetPCP and PCP with specific primers (Table 1). Expression vectors coding for FLAG-tagged

HEV-1 MetPCP and PCP were then generated using the Gateway cloning procedure (Invitrogen) as described above. The ORF1 nucleotide sequence of the HEV-1 strain has been deposited in the GenBank database under accession number MH976520. The amino acid sequences of the MetPCP and PCP fragments from this HEV-1 strain are 99% identical to the one of the Sar55 HEV-1 strain.

The p3Flag-V plasmid coding for the V protein of a Schwarz strain of measles virus (MV) fused to a 3xFLAG tag [45] have been described previously.

2.3. *Reagents and antibodies*

Recombinant human IFN-β1a was purchased from PBL Interferon Source and recombinant human IFN-γ from PeproTech. The mouse anti-actin monoclonal antibody (clone AC-40) and the mouse anti-FLAG (clone M2) were from Sigma-Aldrich. Polyclonal antibodies against STAT1 (06-501), phospho-STAT1 (Tyr701) (07-307) and phospho-STAT2 (Tyr 689) (07-224) were from Millipore. The rabbit polyclonal antibody against STAT2 (SC-476) was from Santa-Cruz Biotechnology.

2.4. *Transfections*

293T cells were transfected with plasmid DNA using JetPRIME (Polyplus transfection, Ozyme) according to the manufacturer's instructions.

2.5. *Cell viability test.*

293T cells were seeded into a 96-well plate ($7.5x10^4$ cells/well) and transfected one day later with the different p3xFLAG constructs. Forty h post-transfection, cells were lysed and cell viability was determined using the CellTiter-Glo® luminescent cell viability assay (Promega) according to the manufacturer's recommendations. This assay is based on ATP quantification as indicator of metabolically active cells.

2.6. *Immunoblot analysis*

293T cells were plated in 6-well plates ($2x10^6$ cells/well) and transfected with 2 µg of the different p3xFLAG constructs. Cells were lysed in RIPA buffer (25 mM Tris HCl pH 8.8, 50 mM NaCl, 0.5% Nonidet P-40 and 0.1% sodium dodecyl sulphate supplemented with cocktails of protease and phosphatase inhibitors) as previously described [47]. Insoluble material was centrifuged at 16,000 g for 20 min at 4°C and discarded. Total protein concentration of the soluble fraction was determined by Micro BCATM Protein assay (Thermo Scientific, Pierce). Equal amount of protein extract was reduced by heating in the presence of β-mercaptoethanol and resolved by 12% sodium dodecyl sulphate-polyacrylamide gel electrophoresis (SDS-PAGE) followed by transfer to nitrocellulose membrane (Hybond-ECL, Amersham). Membranes were blocked with phosphate-buffered saline (PBS) containing 5% dry milk and 0.05% Tween-20. The membrane was then incubated with the required dilution of specific antibodies. Bound primary antibodies were detected using horseradish peroxidase-conjugated anti-rabbit or anti-mouse secondary antibodies (Pierce) and an enhanced luminol-based chemiluminescent detection system. Band intensity was measured on scanned immunoblot images using the ImageJ software.

2.7. Reporter gene assay

293T cells ($4x10^5$ cells/well) were seeded in 24-well plates. 24 h later, cells were transfected with 100 ng of firefly luciferase ISRE reporter plasmid containing the ISRE enhancer element upstream of the firefly luciferase gene (pISRE-Luc, Clontech), 10 ng of the Renilla luciferase cytomegalovirus (CMV) reporter plasmid (pCMV-Luc) for normalization of the data and 250 ng of a plasmid coding for ORF1 or its domains of interest fused to a 3xFLAG tag at their amino-terminal end or 250 ng of a pCINeo-3×FLAG empty vector as negative control or 250 ng of a plasmid coding for MV-V fused to a 3xFLAG tag as positive control. Forty h later, the supernatant was removed and replaced with fresh complete medium containing 1,000 IU/ml of IFN-β. Seven h later, cells were lysed in passive lysis buffer (Promega). Firefly and renilla luciferase activity was determined using the Bright-Glo™ luciferase assay system (Promega) and the Renilla-Glo™ luciferase assay system (Promega), respectively. The normalized luciferase activity was calculated for each sample by dividing the firefly luciferase activity by the renilla luciferase activity.

2.8. RNA extraction, reverse transcription (RT) and real-time quantitative PCR (RT-qPCR)

293T cells ($2x10^6$ cells/well) were transfected with 2 µg of a pCINeo-3×FLAG empty vector or a plasmid coding for MetPCP, PCP or MV-V fused to a 3xFLAG tag. Forty h post-transfection, cells were stimulated for 6 h with 500 UI/ml of IFN-β. Total RNA was extracted using the RNeasy minikit (Qiagen) including a digestion step on column with DNase I (Qiagen). A second digestion step was performed using a TURBO DNase (Ambion) and the RNA cleaned up on a column using the RNeasy minikit (Qiagen). RT was done using 500 ng of RNA with PrimeScript Reverse Transcriptase (Takara Bio Inc.) according to the manufacturer's instruction. RT-qPCR was performed on 2 µl of cDNA using the SYBR Green Master Mix kit (Roche) and specific primers (Table 1). A LightCycler 96 apparatus (Roche) was used for sample analysis. Samples were denatured for 15 min at 95°C, then DNA was amplified with 40 cycles at 95°C for 30 s, 60°C for 30 s and 72°C for 30 s. The final extension was followed by cooling at 40°C for 30 s. Relative quantification was realized using the 2-ΔΔCT method [48]. Glyceraldehyde 3-phosphate dehydrogenase (GAPDH) was used as endogenous control for normalization. The mean ΔCT obtained in non-stimulated cells transfected with the empty vector was used as the calibrator.

2.9. Immunostaining and fluorescent microscopy

293T cells ($3.5x10^5$ cells/well) were seeded onto 12-mm-diameter coverslips previously coated with poly-D-lysine (Sigma-Aldrich) in 24-well plates and transfected with 250 ng of a pCINeo-3×FLAG empty vector (EV) or a plasmid coding for ORF1, MetPCP, PCP, X, Y or MV-V fused to a 3xFLAG tag. 24 h later, cells were treated or not with IFN-β or –γ for 30 min, washed with PBS and fixed with 4% paraformaldehyde in PBS. Cells were permeabilised with 0.2% Triton X-100 in PBS and incubated in blocking buffer (0.5% BSA in PBS). The appropriate dilution of primary antibodies was then added for 1 h at room temperature. Cells were then washed several times in PBS and DyLightTM 488 anti-mouse and DyLightTM 550 anti-rabbit secondary antibodies (Thermo Scientific) were used to detect bound primary antibodies. Samples were mounted in Mowiol containing 4,6- diamidine-2-phenylindole dihydrochloride (DAPI) (Sigma-Aldrich). Microscopy was carried out with an Axio observer Z1 fluorescent microscope (Zeiss) and images were acquired using the Zen 2012 software.

2.10. Statistical analyses

Unpaired t test or an unequal variances t test were used to analyse the data. Differences were considered to be significant if the P value was < 0.05.

3. Results

3.1. Expression of full-length and individual domains of HEV ORF1.

Sequences coding for full-length ORF1 and the MetPCP, Y, PCP and X domains of a HEV-3f strain were identified according to a previous computer-based analysis [3], amplified and inserted in an expression vector downstream and in frame of a sequence coding for a 3xFLAG tag (Figure 1a). Expression of the different constructs was confirmed in 293T cells by immunoblotting (Figure 1b). These human embryonic kidney cells were used as they give high transfection efficiency that cannot be reached in hepatic cell lines. Bands corresponding to the expected molecular weight of FLAG-ORF1 (192 kDa), FLAG-Y (31 kDa), FLAG-X (26 kDa) and FLAG-MetPCP (72 kDa) were detected. Bands of lower molecular weight were also observed for FLAG-ORF1 and FLAG-MetPCP, suggesting cleavage or degradation of these proteins. In contrast, bands corresponding to higher molecular weights than the one expected (23 kDa) were detected for FLAG-PCP, suggesting post-translational modification and/or dimerization of the viral protein (Figure 1b).

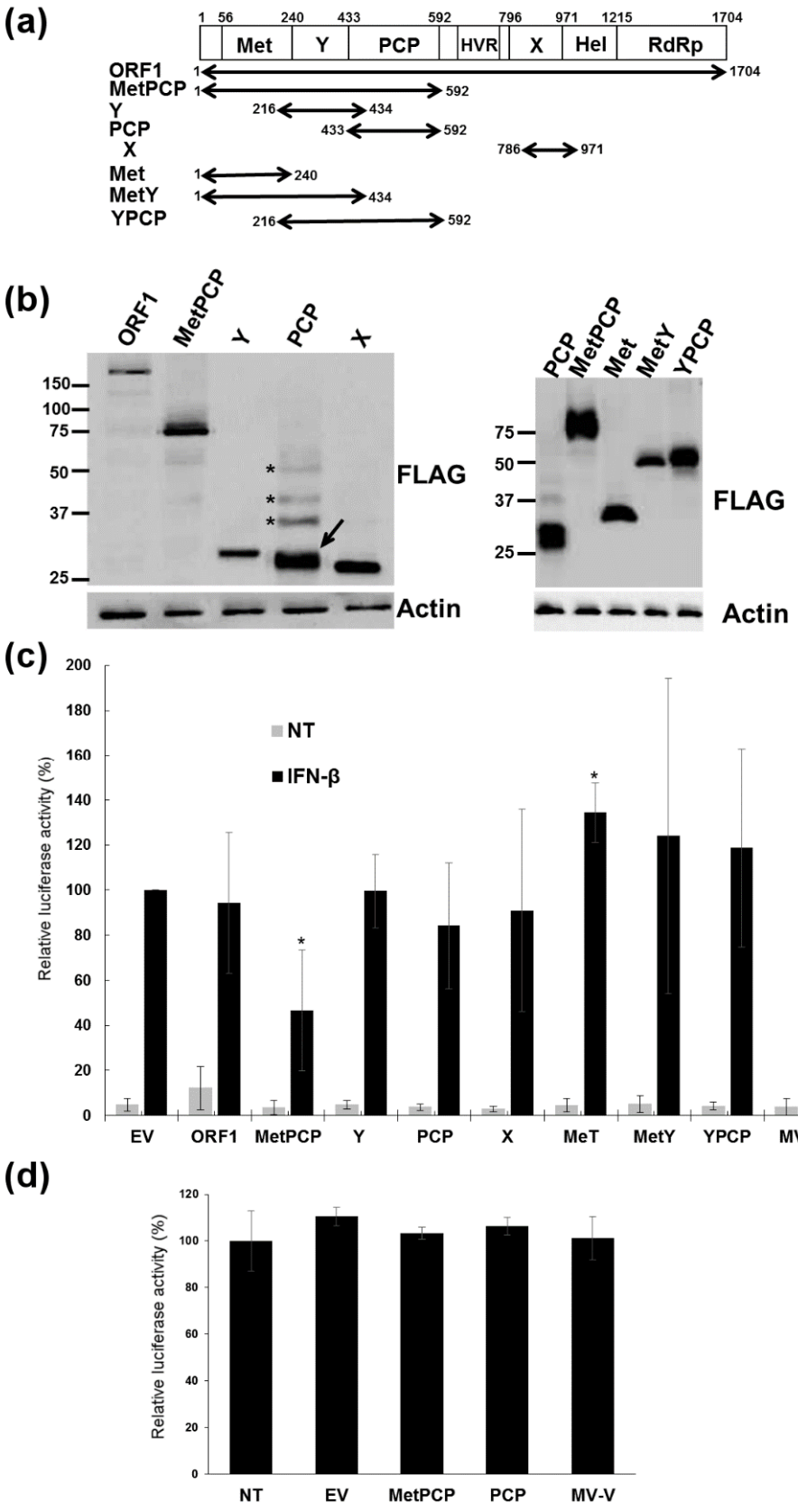

Figure 1. Effect of the expression of full-length HEV ORF1 and several of its domains on ISRE promoter activation. (**a**) Schematic representation of the different domains of HEV ORF1. Met, methyltransferase domain; Y, Y domain; PCP, papain-like cysteine protease; HVR, hypervariable region; X, macro domain; Hel, helicase domain; RdRp, RNA-dependent RNA polymerase. The position of the different putative

functional domains present in the ORF1 amino acid sequence of the HEV-3 strain used in this study is indicated. The different fragments of ORF1 that were cloned and expressed in 293T cells are represented by arrows. (**b**) Expression of FLAG-tagged full-length and domains of ORF1 in 293T cells detected by immunoblotting using an anti-FLAG antibody. Bands corresponding to PCP (arrow) and PCP products of higher molecular weight (asterisks) are indicated. Actin served as loading control. Cells were lysed 18 h post-transfection. (**c**) Effect of full-length ORF1, MetPCP, Y, PCP, macro domain (X), Met, MetY and YPCP on ISRE promoter activation. 293T cells were transfected with pISRE-Luc, pCMV-Luc and a pCINeo-3×FLAG empty vector (EV) or a plasmid coding for MV-V, ORF1, MetPCP, Y, PCP or X. Forty h later, cells were treated or not (NT) with IFN-β for 7 h and lysed to determine firefly and renilla luciferase activities. Mean ratios between firefly and renilla luciferase activities were calculated and are presented as percentages of the treated EV control (± standard deviations). Results shown represent the mean of 4 independent experiments performed in triplicate. *, $P < 0.05$; ***, $P < 0.0005$ compared to EV control for treated samples (unequal variances t tests). (**d**) Cell viability assays at 40 h post-transfection. 293T cells were transfected or not (NT) with a pCINeo-3×FLAG empty vector (EV) or a plasmid coding for MetPCP, PCP or MV-V fused to a 3xFLAG tag. Forty h after transfection, cells were lysed and cell viability determined using a luminescent-based assay. Luciferase activities (± standard deviations) are expressed as percentage relative to non-transfected cells. No significant difference was found between the cells transfected with the pCINeo-3×FLAG empty vector and the one transfected with the plasmid coding for MetPCP, PCP or MV-V. Results are representative of one experiment and were reproduced in 3 independent experiments performed in triplicate.

3.2. MetPCP of HEV ORF1 inhibits the IFN-I response

To assess the ability of the different HEV ORF1 products to interfere with the IFN-I response, we first examined their effect on ISRE promoter activation using a luciferase reporter assay. 293T cells were transfected with an ISRE-reporter plasmid (pISRE-Luc), a control vector (pCMV-Luc) to normalize for transfection and a pCI-Neo empty vector (EV) or plasmids coding for ORF1, MetPCP, Y, PCP or X. Cells were treated 40 h later with IFN-β for 7 h. As a positive control, cells were transfected with a plasmid coding for the V protein of the Schwarz strain of measles virus (MV-V) fused to a FLAG tag at its amino-terminal. This viral protein inhibits the IFN-I response by interacting with STAT1 and JAK1 and interfering with STAT1 and TYK2 phosphorylation [45]. As shown in Figure 1c, the expression of MetPCP was able to inhibit significantly ISRE promoter activation after stimulation with IFN-β. This inhibition was not due to a cytotoxic effect of the viral protein as transfection of the construct coding for MetPCP for 40 h did not affect cell viability (Figure 1d). In contrast, no significant inhibition was detected when PCP alone was expressed. It is interesting to note that both MetPCP and PCP were able to inhibit significantly IFN-β promoter activity after stimulation of the RLR pathway in a luciferase reporter assay (data not shown). This result is in agreement with previous findings showing that PCP from HEV-1 ORF1 is an inhibitor of the RLR pathway [35] and suggests that the PCP domain expressed in our study is functional. ORF1 had no impact on ISRE promoter activation in our assay but the relatively low expression of full-length ORF1 and/or a lack of processing of the polyprotein in 293T cells (Figure 1b) might have masked a putative inhibitory effect. To determine whether the entire MetPCP product is necessary to inhibit ISRE promoter activation, we also tested the effect of Met, MetY and YPCP of HEV ORF1 on ISRE promoter activity using the same luciferase reporter assay (Figure 1a-c). As shown in Figure 1C, expression of

Met alone or MetY or YPCP had no effect on ISRE promoter activation, suggesting that expression of the amino-terminal region of ORF1 containing the Met, Y and PCP domains is necessary to inhibit the signalling pathway triggered by IFN-I.

To further confirm the effect of MetPCP as an antagonist of the IFN-I response, we examined the effect of the viral protein on the level of expression of 3 ISG mRNAs after IFN-β treatment by RT-qPCR (Figure 2a-c). 293T cells were transfected with an empty vector or a plasmid coding for MV-V, PCP or MetPCP for 40 h before stimulation with IFN-β for 6 h. We found that, following IFN-β treatment, expression of MetPCP and, as expected [45], MV-V were able to significantly down-regulate the mRNA levels of ISG56 (Figure 2a), melanoma differentiation-associated protein 5 (MDA5) (Figure 2b) and 2′, 5′-oligoadenylate synthetase 1 (OAS1) (Figure 2c). These results confirm our previous observation (Figure 1c) that MetPCP, but not PCP alone, is able to counteract the IFN-I response.

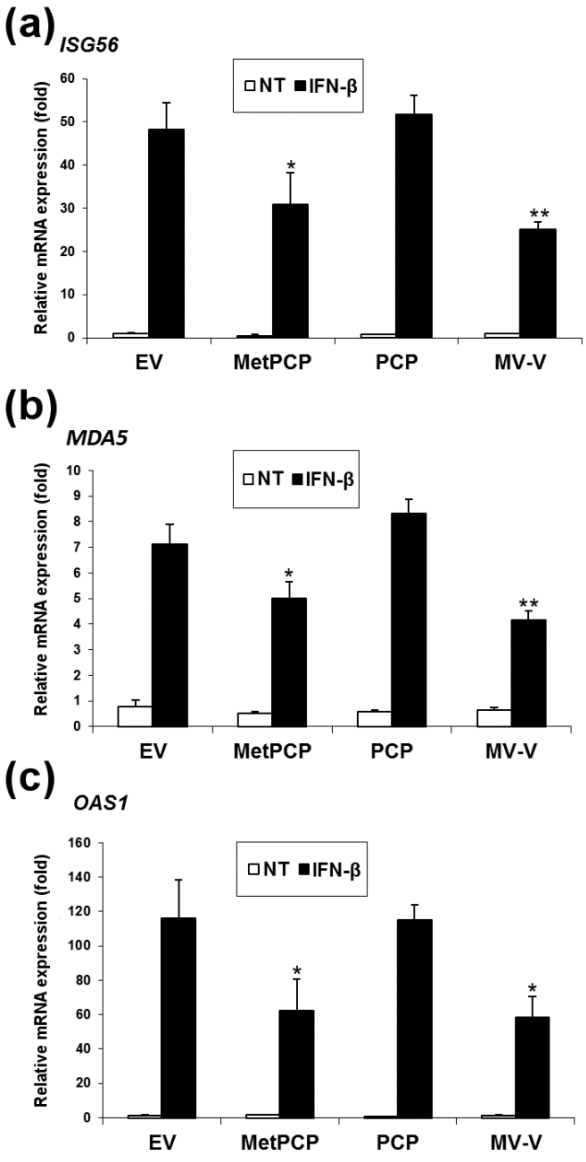

Figure 2. Expression of MetPCP of HEV ORF1 downregulates mRNA levels of several ISGs following IFN-β treatment. (**a-c**) 293T cells were transfected with a pCINeo-3×FLAG empty vector (EV) or a plasmid

coding for MetPCP, PCP or MV-V fused to a 3xFLAG tag. Forty h post-transfection, cells were stimulated or not (NT) with 500 UI/ml of IFN-β for 6 h. Total RNA was extracted and expression of the mRNA coding for ISG56 (**a**), MDA5 (**b**) and OAS1 (**c**) were measured by RT-qPCR. GAPDH was used as reference gene. Data are presented as fold induction (± standard deviations) relative to the non-stimulated EV control. Results are representative of one experiment and were reproduced in 2 independent experiments performed in triplicate. *, $P < 0.05$; **, $P < 0.005$ compared to EV control for treated samples (unpaired t tests).

3.3 MetPCP of HEV ORF1 interferes with the JAK/STAT pathway after IFN-β treatment

To better understand the mechanisms involved in the inhibition of the IFN-I response by MetPCP, we examined whether the viral protein is able to interfere with the JAK/STAT pathway. First, we assessed the ability of MetPCP to modulate STAT1 nuclear translocation after IFN-β stimulation by immunofluorescence. In the absence of IFN treatment, STAT1 was localized mainly in the cytoplasm of 293T cells transfected with an empty vector or plasmids coding for FLAG-tagged MetPCP, PCP or MV-V (Figure 3a). IFN-β treatment led to the nuclear translocation of STAT1 in around 85% of cells transfected with an empty vector or a plasmid coding for PCP (Figure 3a and 3B). In contrast, STAT1 translocated into the nucleus of around 65% of cells expressing MetPCP (Figure 3b). In the remaining cells, STAT1 distribution remained diffuse in the cytoplasm (Figure 3a), suggesting that MetPCP interferes with STAT1 nuclear translocation. As expected, expression of MV-V inhibited STAT1 translocation into the nucleus upon IFN-β treatment (Figure 3a and 3b).

Peer-reviewed version available at Viruses 2018, 10, 726; doi:10.3390/v10120726

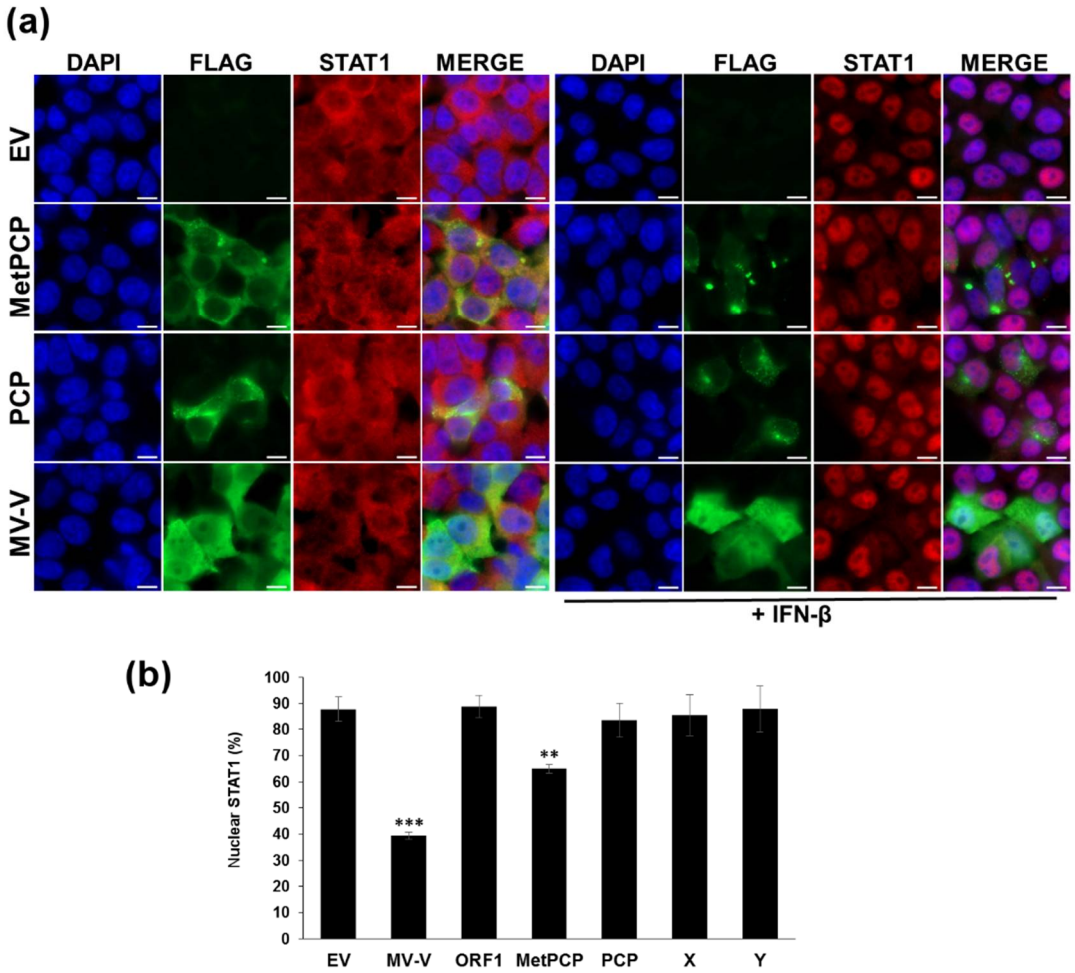

Figure 3. Expression of MetPCP of HEV ORF1 decreases STAT1 nuclear translocation upon IFN-β treatment. (**a**) 293T cells were transfected with a pCINeo-3×FLAG empty vector (EV) or a plasmid coding for MetPCP, PCP or MV-V fused to a 3xFLAG tag. Twenty four h post-transfection, cells were stimulated or not for 30 min with 1000 UI/ml of IFN-β. Cells were then washed, fixed and stained with primary antibodies raised against STAT1 and FLAG, followed by fluorescent dye-conjugated secondary antibodies. Intracellular localization of DAPI-stained nuclei (blue), FLAG (green) and STAT1 (red) was visualized by microscopy (magnification, x630). Scale bars, 10 µm. (**b**) STAT1 localization was visualized after immunostaining as described in (a) in 293T cells transfected with a pCINeo-3×FLAG empty vector (EV) or a plasmid coding for ORF1, MetPCP, PCP, X, Y or MV-V fused to a FLAG tag. For each condition, STAT1 localization was determined in 58 to 181 cells expressing the corresponding FLAG-tagged protein (except for the EV control for which 356 to 384 cells were randomly assessed). The mean percentage (± standard deviation) of cells showing a predominant nuclear localization of STAT1 from 3 independent experiments is shown. **p<0.005 ; ***p<0.0005 compared to EV control for treated samples (unpaired t tests).

3.4. MetPCP of HEV ORF1 inhibits STAT1 but not STAT2 phosphorylation after IFN-β treatment

To investigate which step of the JAK/STAT pathway is targeted by MetPCP, we then assessed the phosphorylation status of STAT1 and STAT2 after IFN-β treatment by immunoblot analysis in 293T cells expressing MetPCP or PCP. Cells expressing MV-V were used as a positive controls. As

shown in Figure 4a and 4b, the level of phosphorylated STAT1 detected after IFN-β treatment was reduced significantly in 293T cells expressing MetPCP in comparison to cells transfected with an empty vector or expressing PCP. No change in the total level of STAT1 was observed in cells expressing MetPCP, indicating that the viral protein did not interfere with the expression or stability of STAT1. Moreover, no significant difference was observed in the level of total and phosphorylated STAT2 (Figure 4a and 4c), suggesting that MetPCP interferes with the activation of STAT1 but not STAT2 following IFN-I treatment.

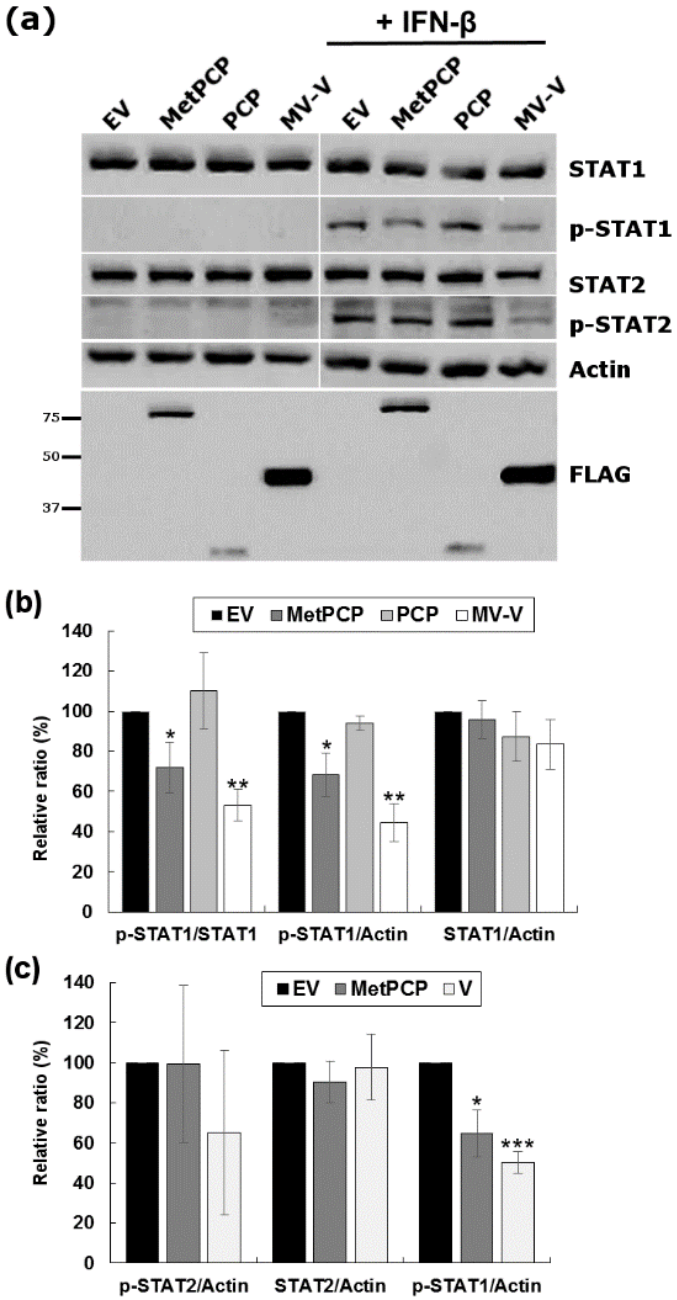

Figure 4. Expression of MetPCP of HEV ORF1 inhibits STAT1 but not STAT2 phosphorylation upon IFN-β treatment. (**a**) 293T cells were transfected with a pCINeo-3×FLAG empty vector (EV) or a plasmid coding

for MetPCP, PCP or MV-V fused to a 3xFLAG tag. Twenty four h post-transfection, cells were stimulated for 30 min with 500 UI/ml of IFN-β. Cell lysates were extracted and used for the detection of FLAG-tagged proteins, total STAT1, phosphorylated STAT1 (p-STAT1), total STAT2 and phosphorylated STAT2 (p-STAT2) by immunoblotting. Actin served as internal control. (**b**) Band intensities were quantified using ImageJ software and relative levels of STAT1, p-STAT1 and actin were determined for each treated sample. Ratio between p-STAT1 and actin, STAT1 and actin, and p-STAT1 and STAT1 were calculated and expressed as relative percentage in comparison to the EV control. (**c**) Band intensities were quantified using ImageJ software and relative levels of STAT2, p-STAT2, p-STAT1 and actin were determined for each treated sample. Ratio between p-STAT2 and actin, STAT2 and actin and p-STAT1 and actin were calculated and expressed as relative percentage in comparison to the EV control. (**b-c**) The mean percentage (± standard deviation) of 4 independent experiments is presented. *, P<0.05; **, P< 0.005; ***p<0.0005 compared to EV control for IFN-treated samples (unequal variances t tests).

3.5. MetPCP of HEV ORF1 inhibits more efficiently the JAK/STAT pathway after IFN-I than IFN-II treatment

We then wanted to determine whether MetPCP has the ability to inhibit the JAK/STAT pathway in response to IFN-II. As IFN-I and –II activation trigger different components of the JAK/STAT pathway, these experiments could help pinpoint at which level of the pathway MetPCP is acting. First, we assessed the effect of MetPCP expression on STAT1 nuclear translocation after IFN-γ stimulation by immunofluorescence. IFN-γ treatment led to the nuclear translocation of STAT1 in around 94% of cells transfected with an empty vector and around 78% of cells expressing MetPCP (Figure 5a), thus suggesting that MetPCP is able to inhibit STAT1 translocation in response to IFN-γ. However, this antagonist effect was less pronounced than the one observed after IFN-β treatment for which 64% of cells expressing MetPCP displayed a predominant localization of STAT1 in the nucleus (Figure 5a). We also assessed the ability of MetPCP to inhibit STAT1 phosphorylation after IFN-II treatment. Cells expressing MetPCP were treated with IFN-γ for 30 minutes and the level of phosphorylated STAT1 was quantified by immunoblotting. As shown in Figure 5b and 5c, no significant inhibition of STAT1 phosphorylation was detected in cells expressing MetPCP following IFN-γ treatment. These results suggest that MetPCP has a limited impact on the JAK/STAT pathway after IFN-II treatment. Similarly to MetPCP, MV-V caused a slight decrease of STAT1 translocation (Figure 5a) and did not inhibit STAT1 phosphorylation (Figure 5b and 5c) after IFN-γ treatment. These results are in agreement with several studies showing that MV-V is more efficient at antagonizing the response to IFN-I in comparison to IFN-II [49–51].

Peer-reviewed version available at Viruses 2018, 10, 726; doi:10.3390/v10120726

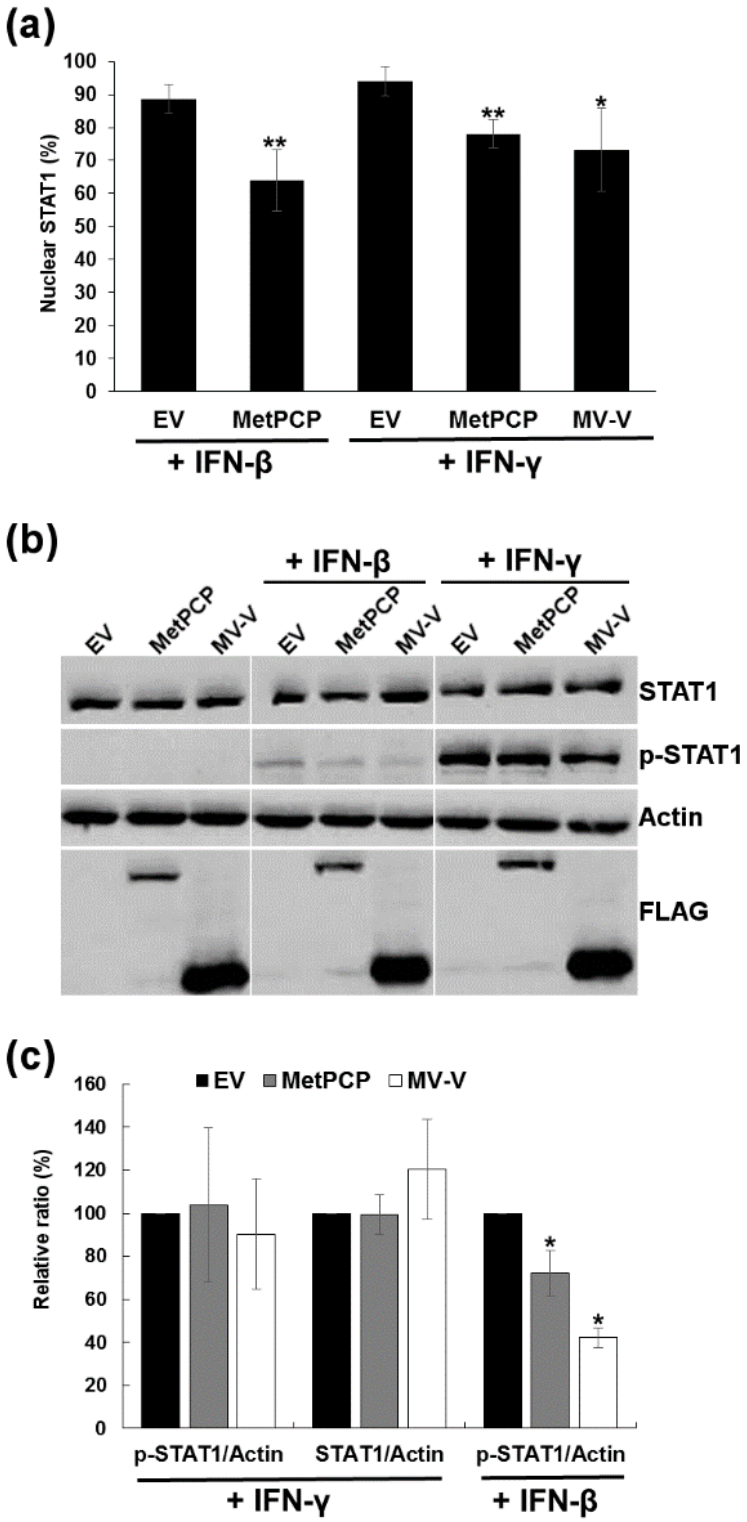

Figure 5. Expression of MetPCP of HEV ORF1 inhibits weakly STAT1 translocation but not STAT1 phosphorylation in response to IFN-II. (**a**) 293T cells were transfected with a pCINeo-3×FLAG empty vector (EV) or a plasmid coding for MetPCP or MV-V fused to a 3xFLAG tag. Twenty four h post-transfection, cells were stimulated for 30 min with 1000 UI/ml of IFN-β or 250 ng/ml of IFN-γ. Cells were then washed, fixed and stained with primary antibodies raised against STAT1 and FLAG, followed by fluorescent dye-conjugated secondary antibodies. STAT1 localization was determined in 64 to 219 cells expressing the corresponding FLAG-tagged protein (except for the EV control for which 305 to 346 cells were randomly

assessed). The mean percentage (± standard deviation) of cells showing a predominant nuclear localization of STAT1 from 4 independent experiments is shown. *p<0.05; **p<0.005 compared to EV control for treated samples (unpaired t tests). (**b**) 293T cells were transfected with a pCINeo-3×FLAG empty vector (EV) or a plasmid coding for MetPCP, PCP or MV-V fused to a 3xFLAG tag. Twenty four h post-transfection, cells were stimulated for 30 mins with 500 UI/ml of IFN-β or 250 ng/ml of IFN-γ. Cell lysates were extracted and used for the detection of FLAG-tagged proteins, total STAT1, phosphorylated STAT1 (p-STAT1) and actin as internal control by immunoblotting. (**c**) Band intensities were quantified using ImageJ software and relative level of STAT1, p-STAT1 and actin were determined for each sample treated with 125 or 250 ng/ml of IFN-γ or 500 UI/ml of IFN-β. Ratio between p-STAT1 and actin and STAT1 and actin were then calculated and expressed as relative percentage in comparison to the EV control. The mean percentage (± standard deviation) of 3 independent experiments is presented. . *p<0.05 compared to EV control (unequal variances t tests).

3.6. The ability of MetPCP of HEV ORF1 to inhibit the JAK/STAT pathway after IFN-I differs between genotypes

We then wondered whether the ability of MetPCP to inhibit the JAK/STAT pathway is genotype-specific and differs between "human only" (HEV-1) and zoonotic (HEV-3) genotypes. To achieve this, the sequences coding for the MetPCP and PCP domains of a HEV-1 strain were cloned and inserted into a 3xFLAG expression vector. We found an amino acid sequence identity of 85% between the MetPCP domains from the HEV-1 and HEV-3 strains cloned in this study and of 69% between the PCP domains. Expression of the ORF1 fragments was then confirmed in 293T cells by immunoblotting (Figure 6a). The effect of the HEV-1 MetPCP and PCP domains on ISRE promoter activation was then assessed using the luciferase reporter assay described above. As shown in Figure 6b, MetPCP from HEV-3 but not HEV-1 was able to inhibit ISRE promoter activation after IFN-β treatment. This difference was not due to a problem of expression of HEV-1 MetPCP as this domain is more efficiently expressed in 293T cells than HEV-3 MetPCP (Figure 6a). In agreement with this result, we also found that the expression of MetPCP from HEV-3 but not HEV-1 inhibited significantly STAT1 nuclear translocation after IFN-β stimulation (Figure 6c). Altogether, these results suggest that the MetPCP domain from HEV-1 is not able to inhibit the JAK/STAT pathway as efficiently as the one from HEV-3 and that differences in the ability of MetPCP to interfere with the JAK/STAT pathway exist between HEV genotypes.

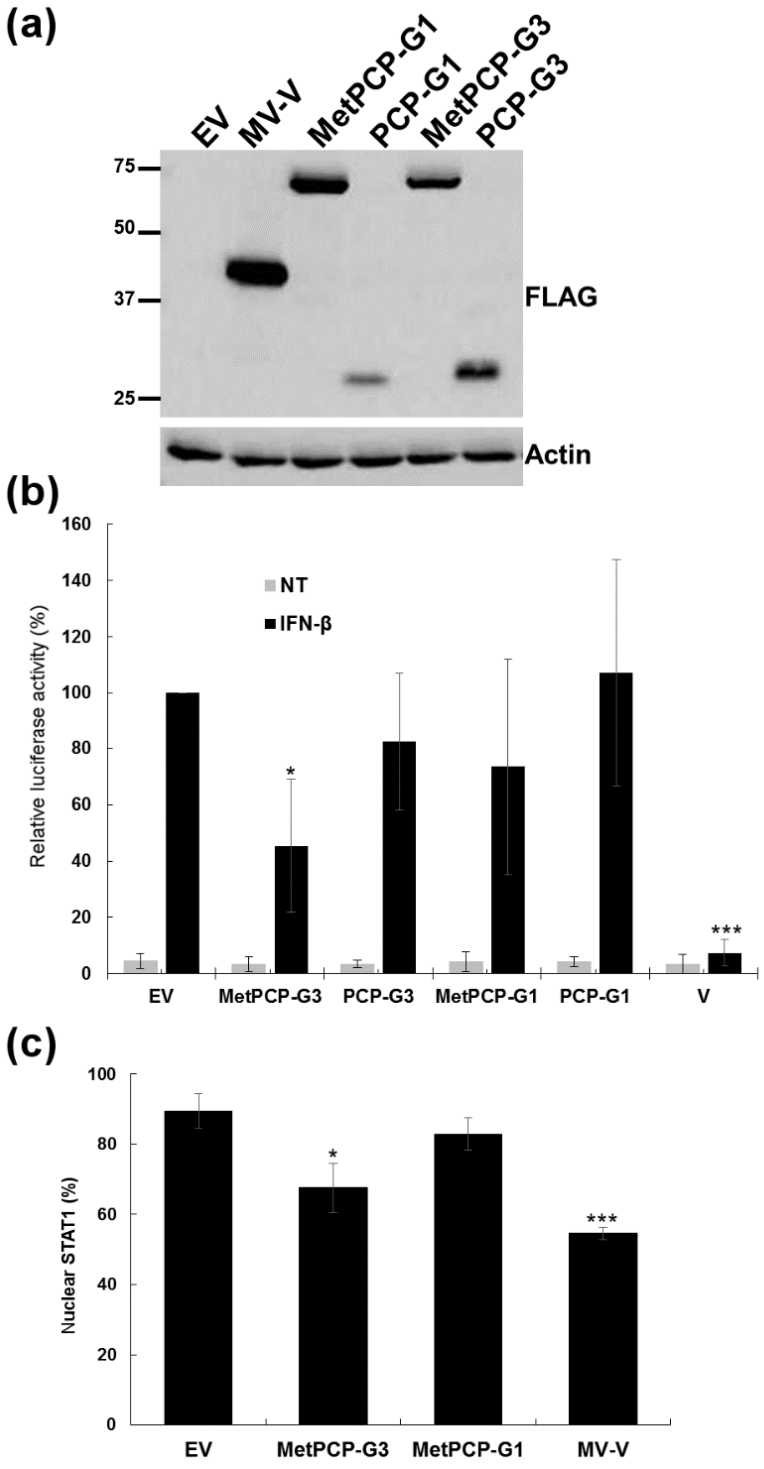

Figure 6. Comparison of the effect of MetPCP from HEV-1 and HEV-3 on the JAK/STAT pathway. (**a**) Expression of FLAG-tagged MetPCP and PCP from a strain of HEV-1 (MetPCP-G1 and PCP-G1) and HEV-3 (MetPCP-G3 and PCP-G3) in 293T cells detected by immunoblotting using an anti-FLAG antibody. Actin served as loading control. Cells were lysed 24 h post-transfection. (**b**) Effect of MetPCP and PCP from HEV-1 and HEV-3 on ISRE promoter activation. 293T cells were transfected with pISRE-Luc, pCMV-Luc and a pCI-Neo empty vector (EV) or a plasmid coding for MV-V, MetPCP-G1, MetPCP-G3, PCP-G1 and PCP-G3. Forty h later, cells were treated or not (-) with IFN-β for 7 h and lysed to determine firefly and renilla luciferase activities. Mean ratios between firefly and renilla luciferase activities were calculated and are presented as percentages of the treated EV control (± standard deviations). Results shown represent the

mean of 5 independent experiments performed in triplicate. *, P < 0.05; ***, P < 0.0005 compared to EV control for treated samples (unequal variances t tests). (**c**) 293T cells were transfected with a pCINeo-3×FLAG empty vector (EV) or a plasmid coding for MetPCP-G3, MetPCP-G1 or MV-V fused to a 3xFLAG tag. Twenty four h post-transfection, cells were stimulated for 30 min with 1000 UI/ml of IFN-β. Cells were then washed, fixed and stained with primary antibodies raised against STAT1 and FLAG, followed by fluorescent dye-conjugated secondary antibodies. STAT1 localization was determined in 70 to 117 cells expressing the corresponding FLAG-tagged protein (except for the EV control for which 311 to 328 cells were randomly assessed). The mean percentage (± standard deviation) of cells showing a predominant nuclear localization of STAT1 from 3 independent experiments is shown. *p<0.05; ***p<0.0005 compared to EV control for treated samples (unpaired t tests).

4. Discussion

Most viruses encode multifunctional viral proteins that counteract the host antiviral response at several steps of the IFN system [52]. Recent studies have reported that the PCP domain, the macrodomain and the Met domain of HEV ORF1 are antagonists of IFN induction [35,36]. The macrodomain was shown to interfere with IRF-3 phosphorylation whereas PCP is able to deubiquitinate components of the RLR pathway such as RIG-I and TANK binding kinase 1 (TBK-1) in 293T cells [35]. Here, we showed that the amino-terminal region of HEV ORF1 is able to inhibit the IFN-I response by targeting the JAK/STAT pathway. Thus, domains of the non-structural polyprotein ORF1 counteract the host IFN system, at the level of IFN induction [35,36] and IFN signalling (our study).

We found that a protein encompassing the predicted Met, Y and PCP domains of HEV ORF1 inhibits ISRE promoter activation and the expression of several ISGs in response to IFN-β. Further investigations revealed that MetPCP interferes with IFN-β-induced STAT1 nuclear translocation and phosphorylation, thus indicating that MetPCP targets the JAK/STAT pathway. Moreover, MetPCP seemed to act specifically on STAT1 activation as STAT2 phosphorylation was not affected by the expression of this ORF1 product. STAT1 is a key component of the JAK/STAT pathway that is targeted by a large number of viral proteins and multiple mechanisms of inhibition have been described [52,53]. Some viral proteins interact directly with STAT1 to block its phosphorylation while others act as phosphatase to dephosphorylate STAT1 or sequester STAT1 in the cytoplasm or induce its degradation [52,53]. Here, we found that MetPCP did not affect total level of STAT1 suggesting that MetPCP is not able to degrade the cellular protein or affect its expression. However, we found that MetPCP was able to inhibit STAT1 phosphorylation more efficiently in response to IFN-β than to IFN-γ, thus suggesting that MetPCP interferes more specifically with one or several components or regulators of the JAK/STAT pathway triggered by IFN-I. Activation of the JAK/STAT pathway by type II IFN involves a specific receptor (IFNGR) and the phosphorylation of JAK1, JAK2 and STAT1 but not TYK2 and STAT2 that are activated by IFN-I only. One can then hypothesize that MetPCP interferes with the recruitment of STAT1 to the IFNAR subunits or with the phosphorylation of STAT1 by TYK2. MetPCP could also interfere with cellular proteins involved in the regulation of IFN-I-driven STAT1 phosphorylation. In addition, it is possible that MetPCP targets several steps of the JAK/STAT pathway and that one target (upstream STAT1 phosphorylation) is specific to the IFN-I response while another (upstream STAT1 translocation) is common to both IFN-I and –II response.

This would explain why we found that MetPCP inhibited significantly the translocation of STAT1 but not its phosphorylation after IFN-II treatment.

We also found that only the ORF1 product containing the predicted functional Met, Y and PCP domains was able to inhibit ISRE promoter activation and not Met, Y or PCP alone or the combination of Met and Y or Y and PCP. A previous study has reported that a putative zinc-finger domain is present in Met (between amino acid 73 and 94) that might be critical for the enzymatic activity of PCP [44]. Many viral cysteine proteases require a zinc-binding finger motif to be catalytically active and/or to function as antagonist of the IFN response. For example, the zinc-finger domain of Nsp1-α of porcine reproductive and respiratory syndrome virus (PRRSV) is critical for the viral protein to inhibit IFN-β synthesis [54]. One can envisage that the enzymatic activity of HEV PCP is dependent on a zinc-finger domain present in Met and is important for the inhibitory action of MetPCP. This would then explain why MetPCP is able to inhibit the JAK/STAT pathway but not, or less efficiently, PCP alone. In future work, it would be interesting to assess the inhibitory effect of MetPCP mutants with a disrupted zinc-binding finger motif to check this hypothesis.

Our results show that the ability of MetPCP to inhibit the JAK/STAT pathway differs according to the HEV genotype involved. This result needs to be further investigated as this difference could explain, at least partially, why distinct pathogenesis and species tropisms are observed between "human only" (HEV-1) and zoonotic (HEV-3) genotypes. Interestingly, a recent paper has suggested that a factor Xa cleavage site is present at amino acid 560 within the PCP domain of HEV-1 strains but is not present in HEV-3 strains [12]. Such differences in the processing of ORF1 between genotypes could affect its function as IFN-I antagonist and need to be better characterised.

4. Conclusion

Until recently, very few studies were undertaken to understand how HEV interacts with the immune system of its host. Data from this study expand our knowledge on the mechanisms evolved by HEV to counteract the IFN response and provide additional evidence that ORF1 plays multiple roles in this evasion strategy. A better understanding of the signalling pathways targeted by HEV proteins to modulate the host antiviral response will help to identify new therapeutic targets and improve the prevention and control of HEV infection. This is critical as no anti-HEV drug has been approved yet and will be particularly relevant for the treatment of chronic cases of hepatitis E in immunosuppressed patients.

Author Contributions: Conceptualization, E.B., V.D. and N.P.; methodology, E.B., V.D., M.P., A.D. and L.M.; formal analysis, E.B., M.P. and V.D.; writing—original draft preparation, V.D.; writing—review and editing, E.B., V.D., M.P., A.D., L.M., N.J. and N.P.; supervision, V.D., N.P. and N.J.; project administration, V.D. and N.P.; funding acquisition, V.D., N.P. and N.J.

Funding: This research was funded by the European Union Seventh Framework Programme PREDEMICS (grant number 278433) and by the Agence Nationale de la Recherche (grant number ANR-16-CE35-0002-01). EB PhD studentship was supported by the DIM Malinf from the Conseil Régional d'Ile-de-France (Grant DIM140079).

Acknowledgments: We thank Jérôme Bouquet, Pierre-Olivier Vidalain, Damien Vitour, Grégory Caignard, Yves Jacob and Frédéric Tangy for providing reagents and for useful discussions.

527 **Conflicts of Interest:** The authors declare no conflict of interest.
528

References

1. Smith, D. B.; Simmonds, P.; International Committee on Taxonomy of Viruses Hepeviridae Study Group; Jameel, S.; Emerson, S. U.; Harrison, T. J.; Meng, X.-J.; Okamoto, H.; Van der Poel, W. H. M.; Purdy, M. A. Consensus proposals for classification of the family Hepeviridae. *J. Gen. Virol.* **2014**, *95*, 2223–2232, doi:10.1099/vir.0.068429-0.
2. Ahmad, I.; Holla, R. P.; Jameel, S. Molecular virology of hepatitis E virus. *Virus Res.* **2011**, *161*, 47–58, doi:10.1016/j.virusres.2011.02.011.
3. Koonin, E. V.; Gorbalenya, A. E.; Purdy, M. A.; Rozanov, M. N.; Reyes, G. R.; Bradley, D. W. Computer-assisted assignment of functional domains in the nonstructural polyprotein of hepatitis E virus: delineation of an additional group of positive-strand RNA plant and animal viruses. *Proc. Natl. Acad. Sci. U.S.A.* **1992**, *89*, 8259–8263.
4. Magden, J.; Takeda, N.; Li, T.; Auvinen, P.; Ahola, T.; Miyamura, T.; Merits, A.; Kääriäinen, L. Virus-specific mRNA capping enzyme encoded by hepatitis E virus. *J. Virol.* **2001**, *75*, 6249–6255, doi:10.1128/JVI.75.14.6249-6255.2001.
5. Sehgal, D.; Thomas, S.; Chakraborty, M.; Jameel, S. Expression and processing of the Hepatitis E virus ORF1 nonstructural polyprotein. *Virol. J.* **2006**, *3*, 38, doi:10.1186/1743-422X-3-38.
6. Paliwal, D.; Panda, S. K.; Kapur, N.; Varma, S. P. K.; Durgapal, H. Hepatitis E virus (HEV) protease: a chymotrypsin-like enzyme that processes both non-structural (pORF1) and capsid (pORF2) protein. *J. Gen. Virol.* **2014**, *95*, 1689–1700, doi:10.1099/vir.0.066142-0.
7. Parvez, M. K. Molecular characterization of hepatitis E virus ORF1 gene supports a papain-like cysteine protease (PCP)-domain activity. *Virus Res.* **2013**, *178*, 553–556, doi:10.1016/j.virusres.2013.07.020.
8. Ropp, S. L.; Tam, A. W.; Beames, B.; Purdy, M.; Frey, T. K. Expression of the hepatitis E virus ORF1. *Arch. Virol.* **2000**, *145*, 1321–1337.
9. Suppiah, S.; Zhou, Y.; Frey, T. K. Lack of processing of the expressed ORF1 gene product of hepatitis E virus. *Virol. J.* **2011**, *8*, 245, doi:10.1186/1743-422X-8-245.
10. Perttilä, J.; Spuul, P.; Ahola, T. Early secretory pathway localization and lack of processing for hepatitis E virus replication protein pORF1. *J. Gen. Virol.* **2013**, *94*, 807–816, doi:10.1099/vir.0.049577-0.
11. Ansari, I. H.; Nanda, S. K.; Durgapal, H.; Agrawal, S.; Mohanty, S. K.; Gupta, D.; Jameel, S.; Panda, S. K. Cloning, sequencing, and expression of the hepatitis E virus (HEV) nonstructural open reading frame 1 (ORF1). *J. Med. Virol.* **2000**, *60*, 275–283.
12. Kanade, G. D.; Pingale, K. D.; Karpe, Y. A. Activities of Thrombin and Factor Xa are essential for replication of Hepatitis E virus and are possibly implicated in the ORF1 polyprotein processing. *J. Virol.* **2018**, doi:10.1128/JVI.01853-17.
13. Doceul, V.; Bagdassarian, E.; Demange, A.; Pavio, N. Zoonotic Hepatitis E Virus: Classification, Animal Reservoirs and Transmission Routes. *Viruses* **2016**, *8*, doi:10.3390/v8100270.
14. Pavio, N.; Meng, X.-J.; Doceul, V. Zoonotic origin of hepatitis E. *Curr Opin Virol* **2015**, *10*, 34–41, doi:10.1016/j.coviro.2014.12.006.

15. Kamar, N.; Abravanel, F.; Lhomme, S.; Rostaing, L.; Izopet, J. Hepatitis E virus: Chronic infection, extra-hepatic manifestations, and treatment. *Clin Res Hepatol Gastroenterol* **2014**, doi:10.1016/j.clinre.2014.07.005.
16. Silvennoinen, O.; Ihle, J. N.; Schlessinger, J.; Levy, D. E. Interferon-induced nuclear signalling by Jak protein tyrosine kinases. *Nature* **1993**, *366*, 583–585, doi:10.1038/366583a0.
17. Gauzzi, M. C.; Velazquez, L.; McKendry, R.; Mogensen, K. E.; Fellous, M.; Pellegrini, S. Interferon-alpha-dependent activation of Tyk2 requires phosphorylation of positive regulatory tyrosines by another kinase. *J. Biol. Chem.* **1996**, *271*, 20494–20500.
18. Krishnan, K.; Yan, H.; Lim, J. T.; Krolewski, J. J. Dimerization of a chimeric CD4-interferon-alpha receptor reconstitutes the signaling events preceding STAT phosphorylation. *Oncogene* **1996**, *13*, 125–133.
19. Platanias, L. C.; Uddin, S.; Colamonici, O. R. Tyrosine phosphorylation of the alpha and beta subunits of the type I interferon receptor. Interferon-beta selectively induces tyrosine phosphorylation of an alpha subunit-associated protein. *J. Biol. Chem.* **1994**, *269*, 17761–17764.
20. Zhao, W.; Lee, C.; Piganis, R.; Plumlee, C.; de Weerd, N.; Hertzog, P. J.; Schindler, C. A conserved IFN-alpha receptor tyrosine motif directs the biological response to type I IFNs. *J. Immunol.* **2008**, *180*, 5483–5489.
21. Abramovich, C.; Shulman, L. M.; Ratovitski, E.; Harroch, S.; Tovey, M.; Eid, P.; Revel, M. Differential tyrosine phosphorylation of the IFNAR chain of the type I interferon receptor and of an associated surface protein in response to IFN-alpha and IFN-beta. *EMBO J.* **1994**, *13*, 5871–5877.
22. Platanias, L. C.; Colamonici, O. R. Interferon alpha induces rapid tyrosine phosphorylation of the alpha subunit of its receptor. *J. Biol. Chem.* **1992**, *267*, 24053–24057.
23. Yan, H.; Krishnan, K.; Greenlund, A. C.; Gupta, S.; Lim, J. T.; Schreiber, R. D.; Schindler, C. W.; Krolewski, J. J. Phosphorylated interferon-alpha receptor 1 subunit (IFNaR1) acts as a docking site for the latent form of the 113 kDa STAT2 protein. *EMBO J.* **1996**, *15*, 1064–1074.
24. Schoggins, J. W.; Rice, C. M. Interferon-stimulated genes and their antiviral effector functions. *Current Opinion in Virology* **2011**, *1*, 519–525, doi:10.1016/j.coviro.2011.10.008.
25. Najjar, I.; Fagard, R. STAT1 and pathogens, not a friendly relationship. *Biochimie* **2010**, *92*, 425–444, doi:10.1016/j.biochi.2010.02.009.
26. Devhare, P. B.; Chatterjee, S. N.; Arankalle, V. A.; Lole, K. S. Analysis of antiviral response in human epithelial cells infected with hepatitis E virus. *PLoS ONE* **2013**, *8*, e63793, doi:10.1371/journal.pone.0063793.
27. Lee, Y. H.; Ha, Y.; Chae, C. Expression of interferon-alpha and Mx protein in the livers of pigs experimentally infected with swine hepatitis E virus. *J. Comp. Pathol.* **2010**, *142*, 187–192, doi:10.1016/j.jcpa.2009.10.025.

28. Moal, V.; Textoris, J.; Ben Amara, A.; Mehraj, V.; Berland, Y.; Colson, P.; Mege, J.-L. Chronic hepatitis E virus infection is specifically associated with an interferon-related transcriptional program. *J. Infect. Dis.* **2013**, *207*, 125–132, doi:10.1093/infdis/jis632.
29. Yu, C.; Boon, D.; McDonald, S. L.; Myers, T. G.; Tomioka, K.; Nguyen, H.; Engle, R. E.; Govindarajan, S.; Emerson, S. U.; Purcell, R. H. Pathogenesis of hepatitis E virus and hepatitis C virus in chimpanzees: similarities and differences. *J. Virol.* **2010**, *84*, 11264–11278, doi:10.1128/JVI.01205-10.
30. Zhang, F.; Qi, Y.; Harrison, T. J.; Luo, B.; Zhou, Y.; Li, X.; Song, A.; Huang, W.; Wang, Y. Hepatitis E genotype 4 virus from feces of monkeys infected experimentally can be cultured in PLC/PRF/5 cells and upregulate host interferon-inducible genes. *J. Med. Virol.* **2014**, *86*, 1736–1744, doi:10.1002/jmv.24014.
31. Yin, X.; Li, X.; Ambardekar, C.; Hu, Z.; Lhomme, S.; Feng, Z. Hepatitis E virus persists in the presence of a type III interferon response. *PLoS Pathog.* **2017**, *13*, e1006417, doi:10.1371/journal.ppat.1006417.
32. Zhou, X.; Xu, L.; Wang, W.; Watashi, K.; Wang, Y.; Sprengers, D.; de Ruiter, P. E.; van der Laan, L. J. W.; Metselaar, H. J.; Kamar, N.; Peppelenbosch, M. P.; Pan, Q. Disparity of basal and therapeutically activated interferon signalling in constraining hepatitis E virus infection. *J. Viral Hepat.* **2016**, *23*, 294–304, doi:10.1111/jvh.12491.
33. Todt, D.; François, C.; Anggakusuma, null; Behrendt, P.; Engelmann, M.; Knegendorf, L.; Vieyres, G.; Wedemeyer, H.; Hartmann, R.; Pietschmann, T.; Duverlie, G.; Steinmann, E. Antiviral Activities of Different Interferon Types and Subtypes against Hepatitis E Virus Replication. *Antimicrob. Agents Chemother.* **2016**, *60*, 2132–2139, doi:10.1128/AAC.02427-15.
34. Dong, C.; Zafrullah, M.; Mixson-Hayden, T.; Dai, X.; Liang, J.; Meng, J.; Kamili, S. Suppression of interferon-α signaling by hepatitis E virus. *Hepatology* **2012**, *55*, 1324–1332, doi:10.1002/hep.25530.
35. Nan, Y.; Yu, Y.; Ma, Z.; Khattar, S. K.; Fredericksen, B.; Zhang, Y.-J. Hepatitis E virus inhibits type I interferon induction by ORF1 products. *J. Virol.* **2014**, *88*, 11924–11932, doi:10.1128/JVI.01935-14.
36. Kang, S.; Choi, C.; Choi, I.; Han, K.-N.; Roh, S. W.; Choi, J.; Kwon, J.; Park, M.-K.; Kim, S.-J.; Myoung, J. Hepatitis E Virus Methyltransferase Inhibits Type I Interferon Induction by Targeting RIG-I. *J. Microbiol. Biotechnol.* **2018**, doi:10.4014/jmb.1808.08058.
37. Lenggenhager, D.; Gouttenoire, J.; Malehmir, M.; Bawohl, M.; Honcharova-Biletska, H.; Kreutzer, S.; Semela, D.; Neuweiler, J.; Hürlimann, S.; Aepli, P.; Fraga, M.; Sahli, R.; Terracciano, L.; Rubbia-Brandt, L.; Müllhaupt, B.; Sempoux, C.; Moradpour, D.; Weber, A. Visualization of hepatitis E virus RNA and proteins in the human liver. *J. Hepatol.* **2017**, *67*, 471–479, doi:10.1016/j.jhep.2017.04.002.
38. Clementz, M. A.; Chen, Z.; Banach, B. S.; Wang, Y.; Sun, L.; Ratia, K.; Baez-Santos, Y. M.; Wang, J.; Takayama, J.; Ghosh, A. K.; Li, K.; Mesecar, A. D.; Baker, S. C. Deubiquitinating and interferon antagonism activities of coronavirus papain-like proteases. *J. Virol.* **2010**, *84*, 4619–4629, doi:10.1128/JVI.02406-09.

39. Fehr, A. R.; Channappanavar, R.; Jankevicius, G.; Fett, C.; Zhao, J.; Athmer, J.; Meyerholz, D. K.; Ahel, I.; Perlman, S. The Conserved Coronavirus Macrodomain Promotes Virulence and Suppresses the Innate Immune Response during Severe Acute Respiratory Syndrome Coronavirus Infection. *MBio* **2016**, *7*, doi:10.1128/mBio.01721-16.
40. Kuri, T.; Eriksson, K. K.; Putics, A.; Züst, R.; Snijder, E. J.; Davidson, A. D.; Siddell, S. G.; Thiel, V.; Ziebuhr, J.; Weber, F. The ADP-ribose-1''-monophosphatase domains of severe acute respiratory syndrome coronavirus and human coronavirus 229E mediate resistance to antiviral interferon responses. *J. Gen. Virol.* **2011**, *92*, 1899–1905, doi:10.1099/vir.0.031856-0.
41. Park, E.; Griffin, D. E. The nsP3 macro domain is important for Sindbis virus replication in neurons and neurovirulence in mice. *Virology* **2009**, *388*, 305–314, doi:10.1016/j.virol.2009.03.031.
42. Sun, Z.; Li, Y.; Ransburgh, R.; Snijder, E. J.; Fang, Y. Nonstructural protein 2 of porcine reproductive and respiratory syndrome virus inhibits the antiviral function of interferon-stimulated gene 15. *J. Virol.* **2012**, *86*, 3839–3850, doi:10.1128/JVI.06466-11.
43. Wang, G.; Chen, G.; Zheng, D.; Cheng, G.; Tang, H. PLP2 of mouse hepatitis virus A59 (MHV-A59) targets TBK1 to negatively regulate cellular type I interferon signaling pathway. *PLoS ONE* **2011**, *6*, e17192, doi:10.1371/journal.pone.0017192.
44. Karpe, Y. A.; Lole, K. S. Deubiquitination activity associated with hepatitis E virus putative papain-like cysteine protease. *J. Gen. Virol.* **2011**, *92*, 2088–2092, doi:10.1099/vir.0.033738-0.
45. Caignard, G.; Guerbois, M.; Labernardière, J.-L.; Jacob, Y.; Jones, L. M.; Infectious Mapping Project I-MAP; Wild, F.; Tangy, F.; Vidalain, P.-O. Measles virus V protein blocks Jak1-mediated phosphorylation of STAT1 to escape IFN-alpha/beta signaling. *Virology* **2007**, *368*, 351–362, doi:10.1016/j.virol.2007.06.037.
46. Mendoza, J.-A.; Jacob, Y.; Cassonnet, P.; Favre, M. Human papillomavirus type 5 E6 oncoprotein represses the transforming growth factor beta signaling pathway by binding to SMAD3. *J. Virol.* **2006**, *80*, 12420–12424, doi:10.1128/JVI.02576-05.
47. Doceul, V.; Chauveau, E.; Lara, E.; Breard, E.; Sailleau, C.; Zientara, S.; Vitour, D. Dual modulation of type I interferon response by Bluetongue virus. *J. Virol.* **2014**, doi:10.1128/JVI.01235-14.
48. Livak, K. J.; Schmittgen, T. D. Analysis of relative gene expression data using real-time quantitative PCR and the 2(-Delta Delta C(T)) Method. *Methods* **2001**, *25*, 402–408, doi:10.1006/meth.2001.1262.
49. Takeuchi, K.; Kadota, S.; Takeda, M.; Miyajima, N.; Nagata, K. Measles virus V protein blocks interferon (IFN)-alpha/beta but not IFN-gamma signaling by inhibiting STAT1 and STAT2 phosphorylation. *FEBS Lett.* **2003**, *545*, 177–182.
50. Chinnakannan, S. K.; Nanda, S. K.; Baron, M. D. Morbillivirus v proteins exhibit multiple mechanisms to block type 1 and type 2 interferon signalling pathways. *PLoS ONE* **2013**, *8*, e57063, doi:10.1371/journal.pone.0057063.

696 51. Ramachandran, A.; Parisien, J.-P.; Horvath, C. M. STAT2 is a primary target for
697 measles virus V protein-mediated alpha/beta interferon signaling inhibition. *J. Virol.*
698 **2008**, *82*, 8330–8338, doi:10.1128/JVI.00831-08.
699 52. Hoffmann, H.-H.; Schneider, W. M.; Rice, C. M. Interferons and viruses: an
700 evolutionary arms race of molecular interactions. *Trends Immunol.* **2015**, *36*, 124–138,
701 doi:10.1016/j.it.2015.01.004.
702 53. Versteeg, G. A.; García-Sastre, A. Viral tricks to grid-lock the type I interferon system.
703 *Curr. Opin. Microbiol.* **2010**, *13*, 508–516, doi:10.1016/j.mib.2010.05.009.
704 54. Shi, X.; Zhang, X.; Wang, F.; Wang, L.; Qiao, S.; Guo, J.; Luo, C.; Wan, B.; Deng, R.;
705 Zhang, G. The zinc-finger domain was essential for porcine reproductive and
706 respiratory syndrome virus nonstructural protein-1α to inhibit the production of
707 interferon-β. *J. Interferon Cytokine Res.* **2013**, *33*, 328–334, doi:10.1089/jir.2012.0100.
708